Supplement of Hydrol. Earth Syst. Sci., 30, 3697–3713, 2026
https://doi.org/10.5194/hess-30-3697-2026-supplement

Hydrology and Earth System Sciences
Open Access
EGU

Supplement of

Uneven decline in the hydrological efficiency of China's natural and plantation forests

Xiao Zhang et al.

Correspondence to: Guodong Jia (jiaguodong@bjfu.edu.cn)

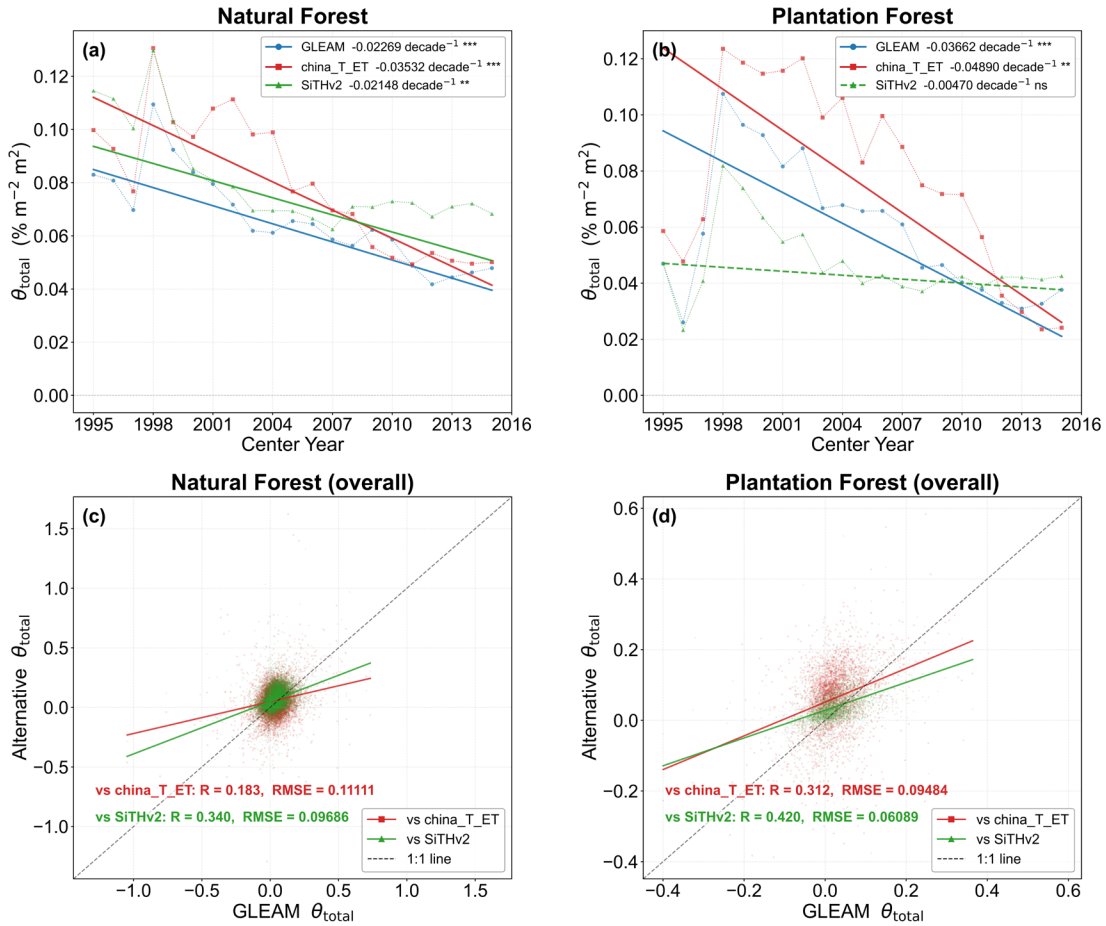

Figure S1. Cross-product robustness check of LAI–transpiration fraction sensitivity (θ_{total}) using three evapotranspiration products. (a, b) Spatial-mean θ_{total} time series for natural forests (NF) and planted forests (PF), respectively, computed from GLEAM, China terrestrial ecosystem transpiration fraction dataset (china_T_ET), and SiTHv2. Data points show the spatial mean of θ_{total} for each 11-year sliding window centered at the indicated year; solid trend lines indicate statistically significant trends ($p < 0.05$, Mann–Kendall test), and dashed lines indicate non-significant trends. Trend magnitudes are Theil–Sen slope estimates (decade^{-1}). (c, d) Pixel-level scatterplots of overall θ_{total} between GLEAM and alternative products for NF and PF, respectively. Each dot represents one 0.1° grid cell; colored solid lines show OLS regression fits, Pearson's R and RMSE are annotated, and the dashed black line indicates the 1:1 reference.

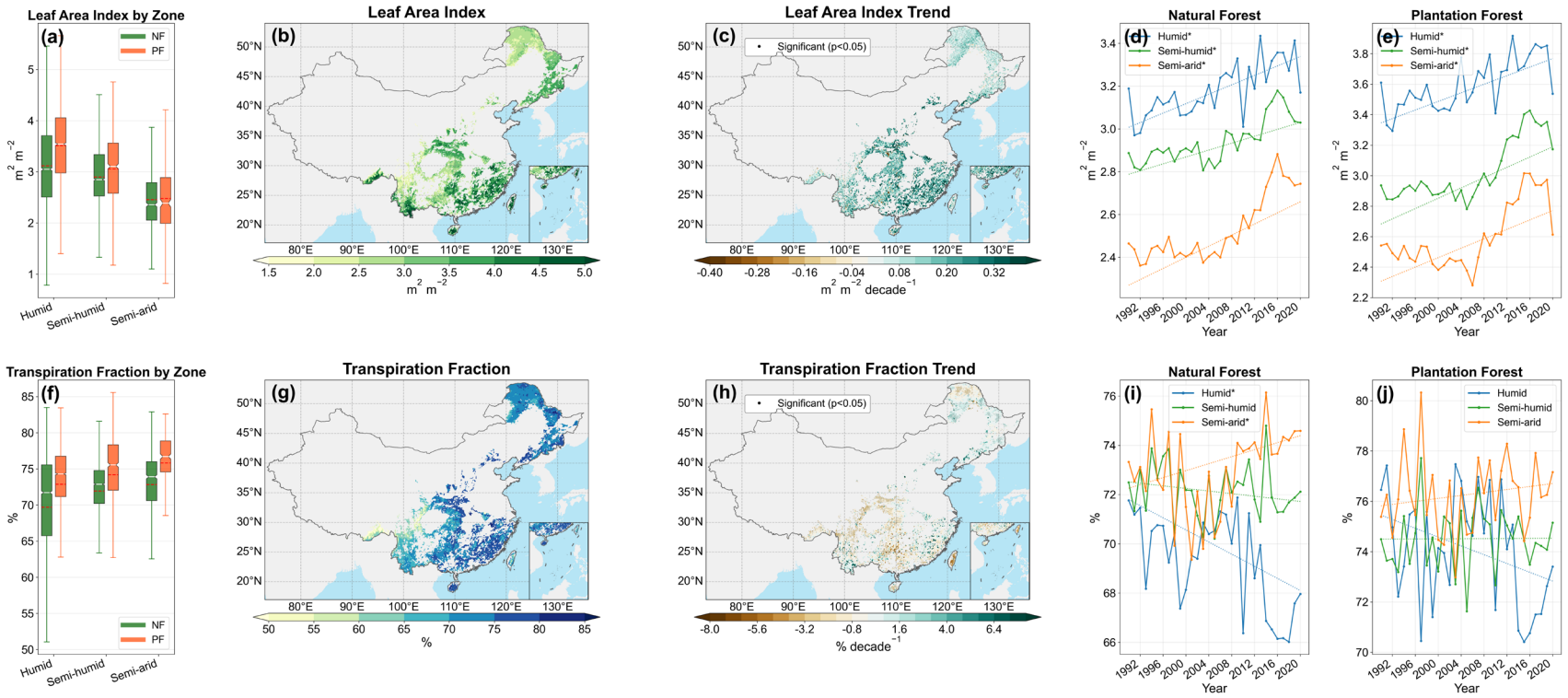

Figure S2. Spatial patterns and temporal trends of Leaf Area Index (LAI; upper row) and Transpiration Fraction (TF; lower row) for China's forests during the 1982–2020 growing season (April–October). (a, f) Box plots of multi-year mean values across three climatic zones (Humid, Semi-humid, Semi-arid), separately for Natural Forest (NF, green) and Plantation Forest (PF, orange). (b, g) Multi-year mean spatial distribution; NF and PF pixels are shown together on the same map. (c, h) Linear trend (decade^{-1}); stippling indicates significant pixels ($p < 0.05$). (d, i) Interannual changes of zone-averaged values for NF with Theil–Sen trend lines (dotted); asterisks (*) in legend denote significant trends (Mann–Kendall, $p < 0.05$). (e, j) Same as (d, i) but for PF.

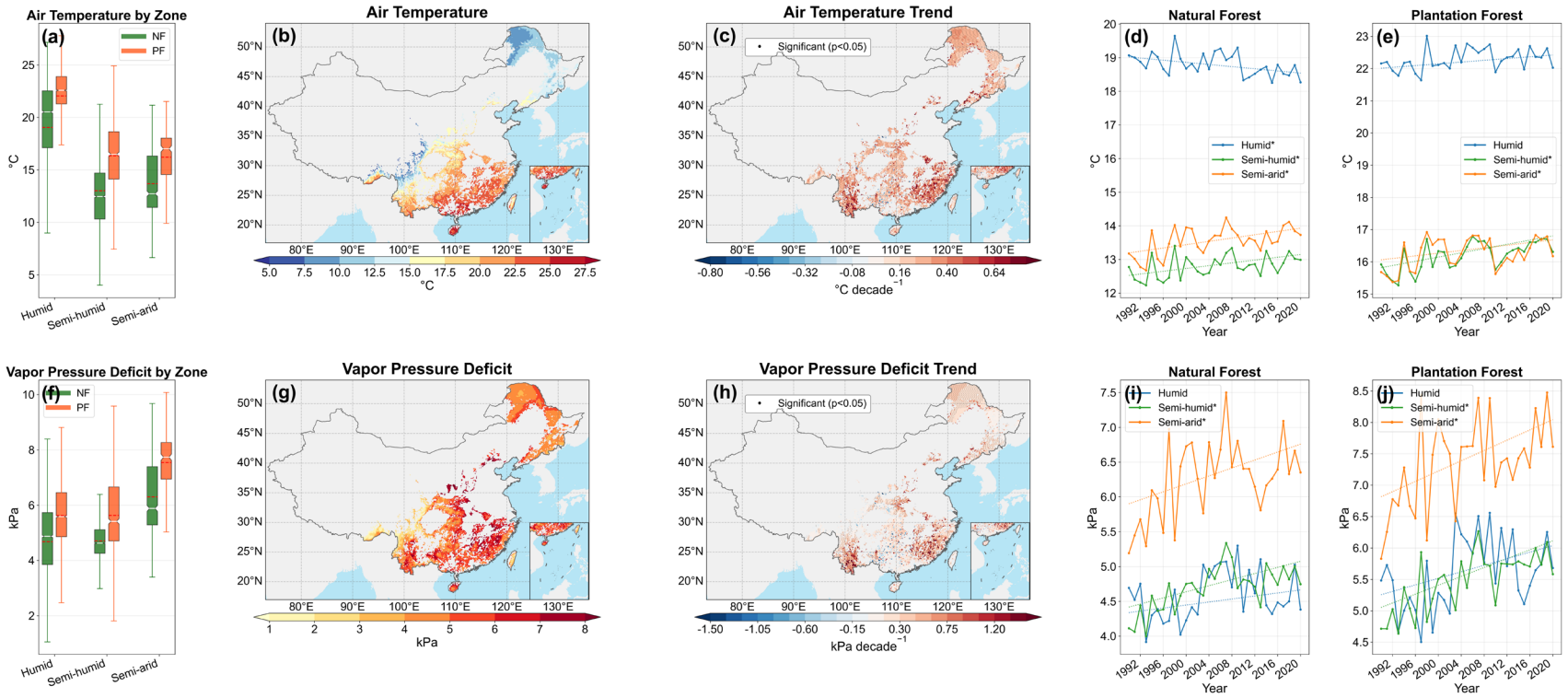

Figure S3. Spatial patterns and temporal trends of Air Temperature (upper row) and Vapor Pressure Deficit (VPD; lower row) for China's forests during the growing season. (a, f) Box plots of multi-year mean values across three climatic zones (Humid, Semi-humid, Semi-arid), separately for Natural Forest (NF, green) and Plantation Forest (PF, orange). (b, g) Multi-year mean spatial distribution; NF and PF pixels are shown together on the same map. (c, h) Linear trend (decade^{-1}); stippling indicates significant pixels ($p < 0.05$). (d, i) Interannual changes of zone-averaged values for NF with Theil–Sen trend lines (dotted); asterisks (*) in legend denote significant trends (Mann–Kendall, $p < 0.05$). (e, j) Same as (d, i) but for PF. Layout and symbology as in Fig. S2.

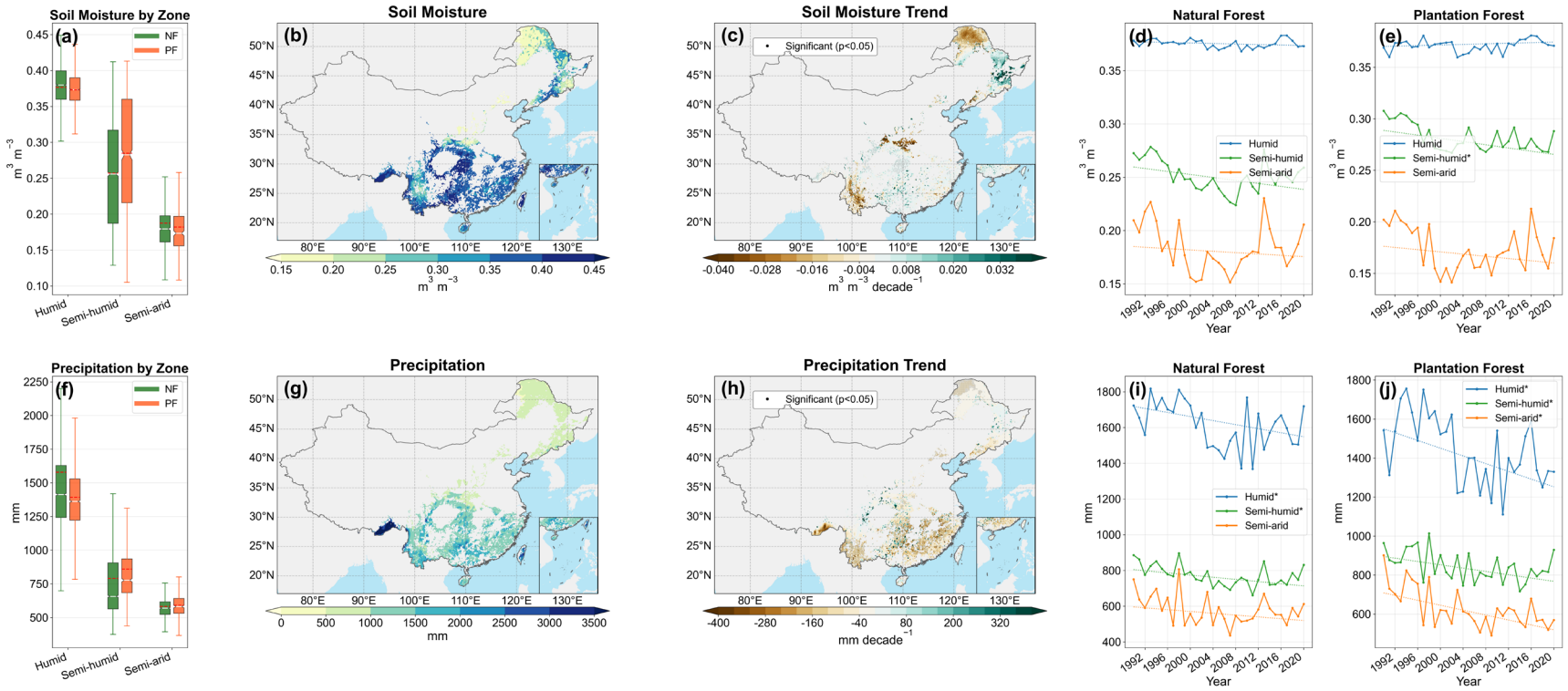

Figure S4. Spatial patterns and temporal trends of Soil Moisture (upper row) and Precipitation (lower row) for China's forests during the growing season. (a, f) Box plots of multi-year mean values across three climatic zones (Humid, Semi-humid, Semi-arid), separately for Natural Forest (NF, green) and Plantation Forest (PF, orange). (b, g) Multi-year mean spatial distribution; NF and PF pixels are shown together on the same map. (c, h) Linear trend (decade^{-1}); stippling indicates significant pixels ($p < 0.05$). (d, i) Interannual changes of zone-averaged values for NF with Theil–Sen trend lines (dotted); asterisks (*) in legend denote significant trends (Mann–Kendall, $p < 0.05$). (e, j) Same as (d, i) but for PF. Layout and symbology as in Fig. S2.

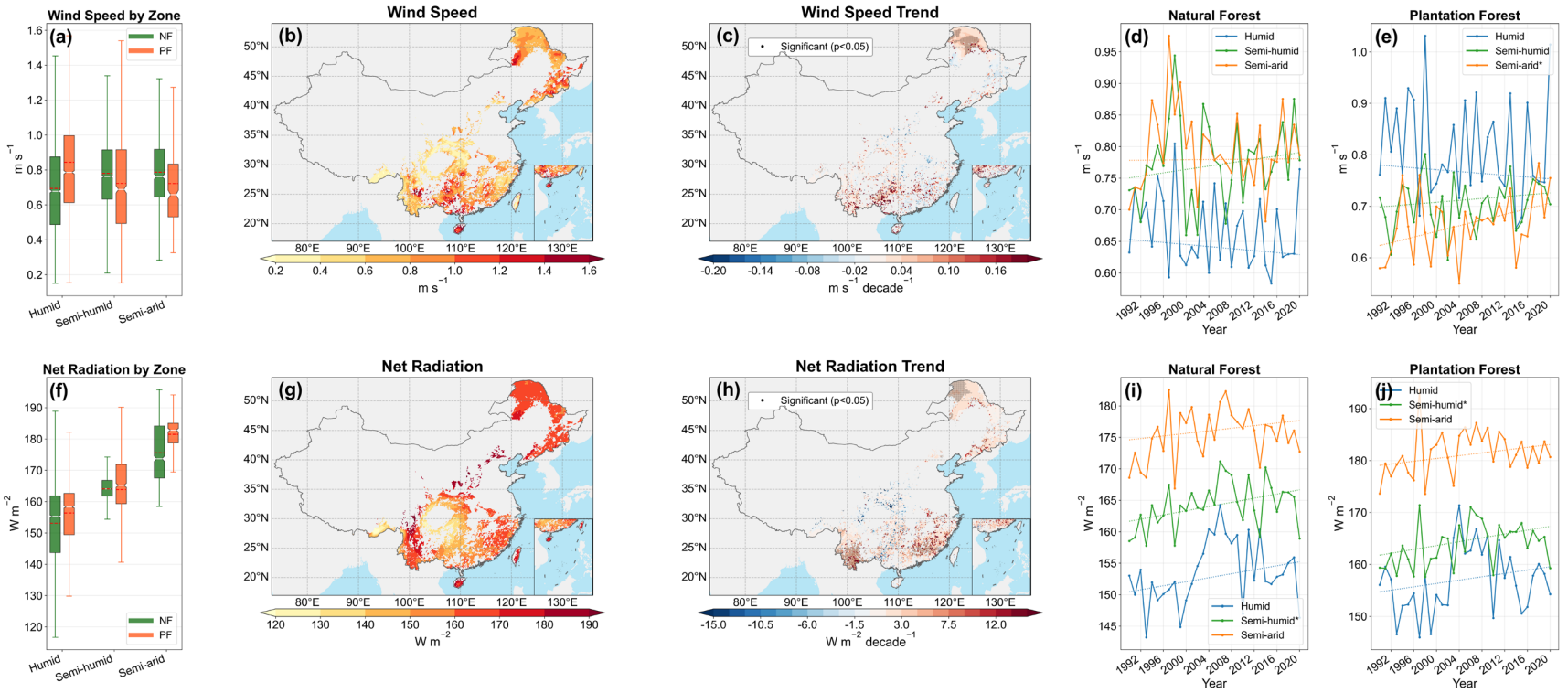

Figure S5. Spatial patterns and temporal trends of Wind Speed (upper row) and Net Radiation (lower row) for China's forests during the growing season. (a, f) Box plots of multi-year mean values across three climatic zones (Humid, Semi-humid, Semi-arid), separately for Natural Forest (NF, green) and Plantation Forest (PF, orange). (b, g) Multi-year mean spatial distribution; NF and PF pixels are shown together on the same map. (c, h) Linear trend (decade^{-1}); stippling indicates significant pixels ($p < 0.05$). (d, i) Interannual changes of zone-averaged values for NF with Theil–Sen trend lines (dotted); asterisks (*) in legend denote significant trends (Mann–Kendall, $p < 0.05$). (e, j) Same as (d, i) but for PF. Layout and symbology as in Fig. S2.

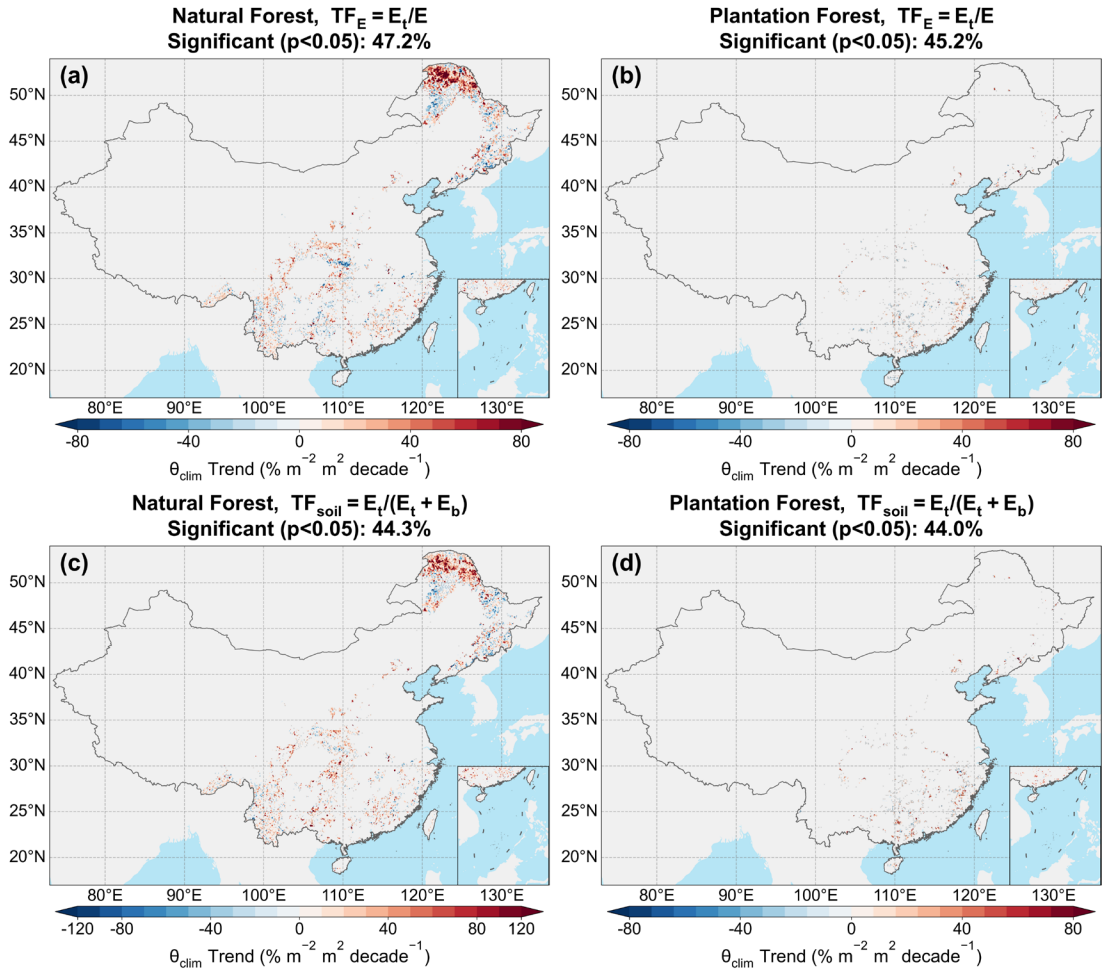

Figure S6. Spatial distribution of the pixel-level interannual trend of θ_{clim} (% m^{-2} m^2 decade^{-1}) under TF$_E$ and TF$_{soil}$ for natural forests (top row) and plantation forests (bottom row). θ_{clim} is the climate-driven component of θ, evaluated at each pixel's time-invariant LAI reference. Trends estimated by Theil–Sen slope; black dots mark significance (Mann–Kendall, $p < 0.05$). Non-zero trends indicate changes in the TF–LAI curve shape itself, independent of LAI movement.

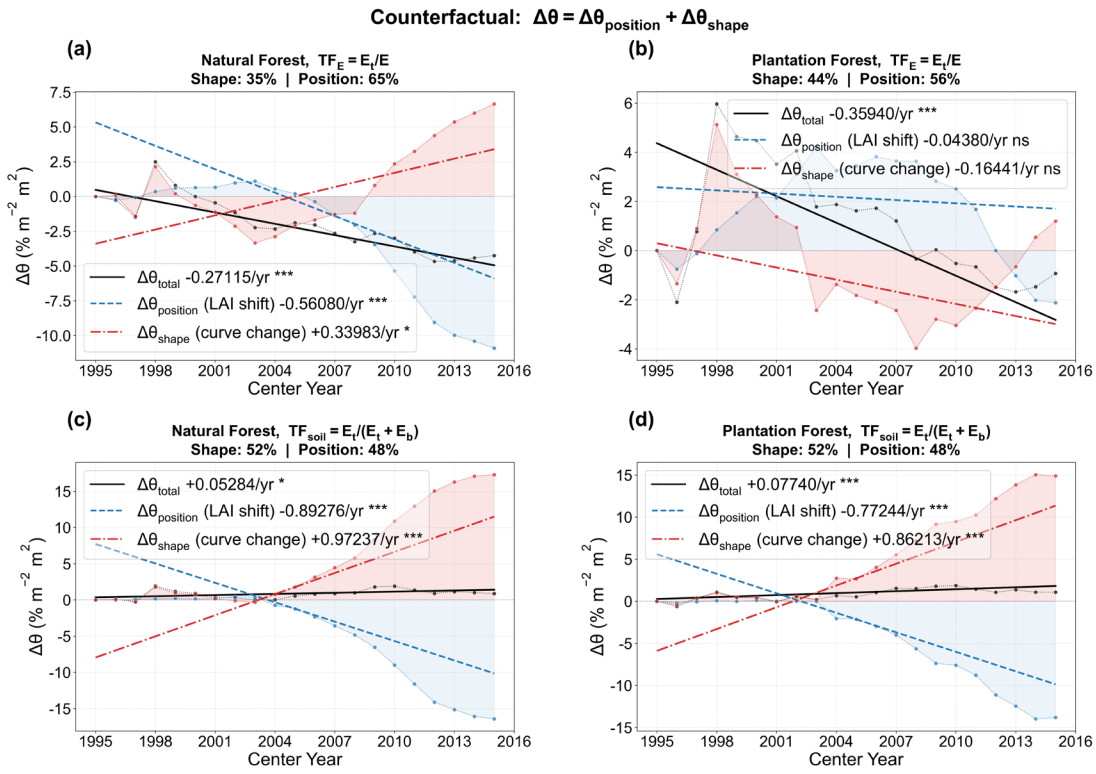

Figure S7. Counterfactual decomposition of $\Delta\theta_{total}$ into a position effect ($\Delta\theta_{position}$, LAI moves along a fixed curve) and a shape effect ($\Delta\theta_{shape}$, the curve itself changes). The null model fixes regression coefficients (a_0, b_0, c_0) at the first window value; the residual (actual minus null) captures curve shape change. Percentages show the relative contribution of each component. Under TF_{soil} the shape effect dominates and reverses the sign relative to the position effect.

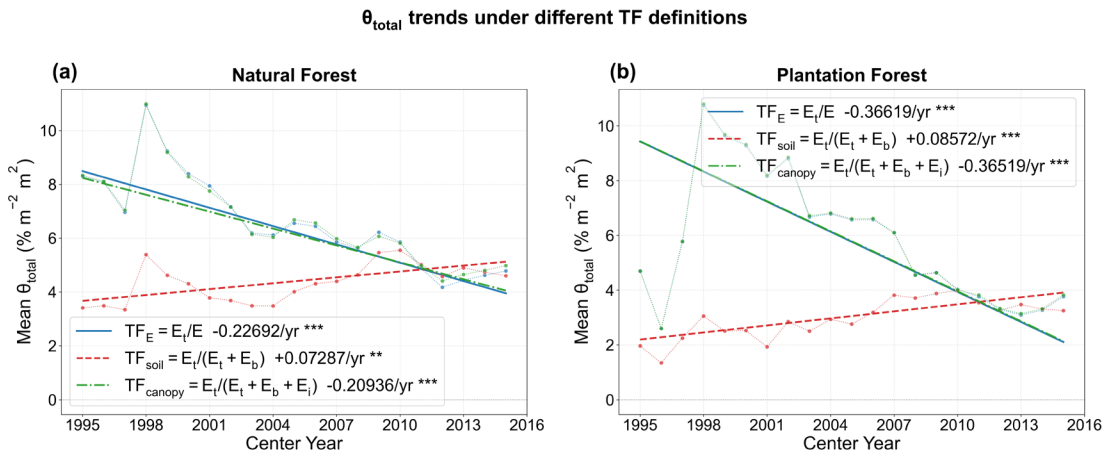

Figure S8. Comparison of spatially averaged θ_{total} time series (% m^{-2} m^2) under three TF definitions—$TF_E = E_t/E$ (blue, solid), $TF_{soil} = E_t/(E_t + E_b)$ (red, dashed), and $TF_{canopy} = E_t/(E_t + E_b + E_i)$ (green, dash-dot)—for natural forests (a) and plantation forests (b). Each data point represents the spatial mean of θ over one 11-year sliding window; Theil–Sen trend lines are overlaid with Mann–Kendall significance (*** $p < 0.001$, ** $p < 0.01$, * $p < 0.05$, ns non-significant).

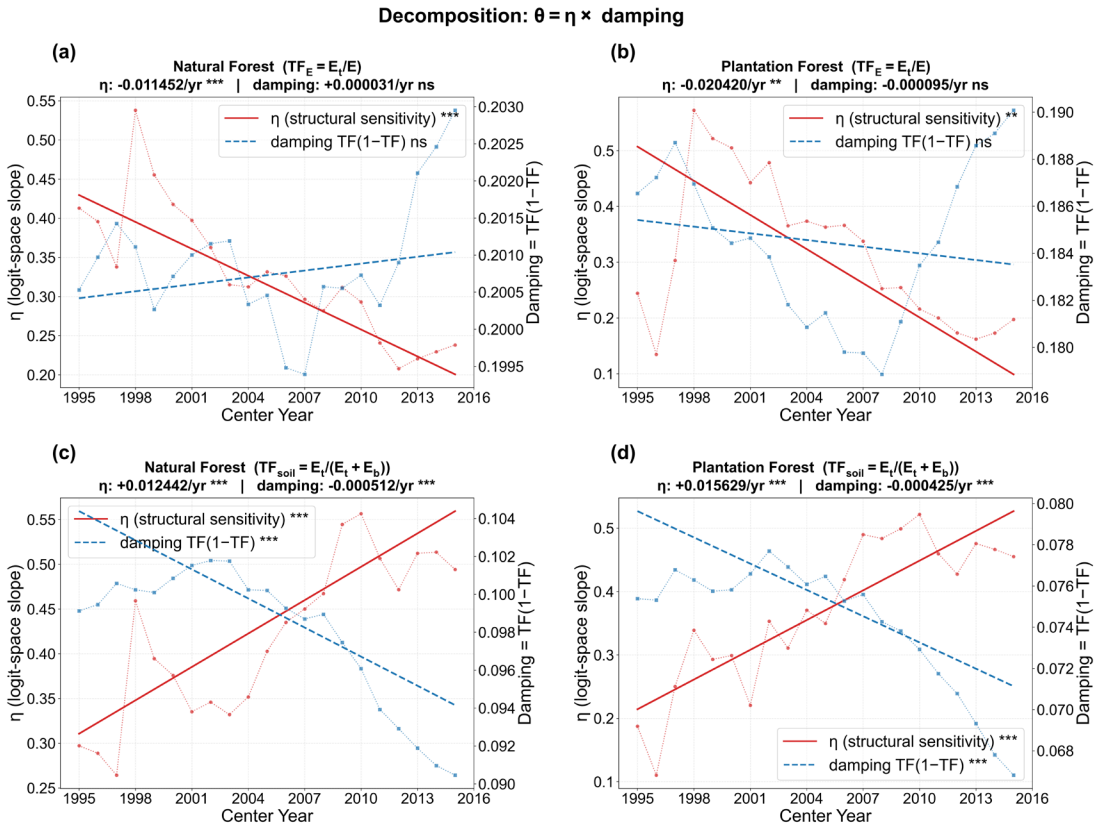

Figure S9. Decomposition of θ into structural sensitivity η and damping factor TF(1 − TF) under TF$_E$ and TF$_{soil}$ for natural (left) and plantation forests (right). θ = η × damping, where η = b + 2c·LAI is the logit-space slope and damping = TF(1 − TF) is the saturation compression factor. Left y-axis (red): η; right y-axis (blue): damping. Theil–Sen slopes and Mann–Kendall significance are annotated.

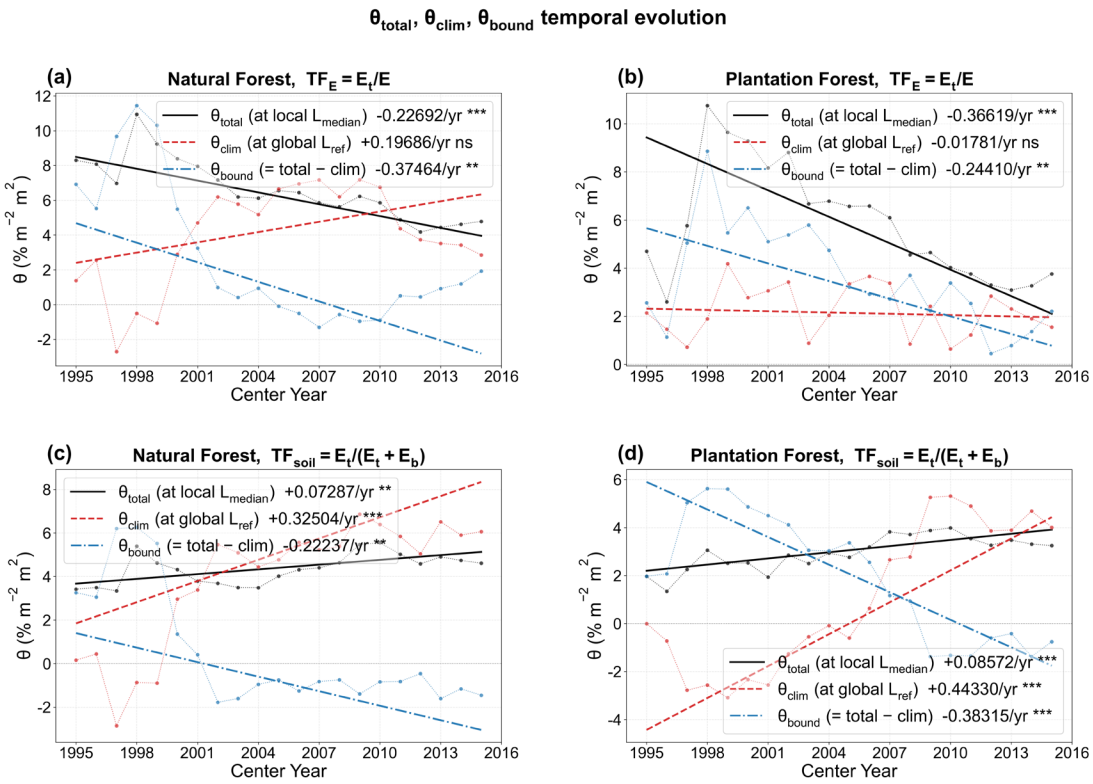

Figure S10. Time series of spatially averaged θ_{total}, θ_{clim}, and θ_{bound} (% m^{-2} m^2) under TF_E and TF_{soil} for natural and plantation forests. θ_{total} (blue) = total LAI–TF sensitivity; θ_{clim} (red) = climate-driven component evaluated at a fixed LAI reference; θ_{bound} (green) = boundary condition component. Theil–Sen trend lines overlaid with Mann–Kendall significance. If the TF–LAI curve were fixed, θ_{clim} would show no trend.

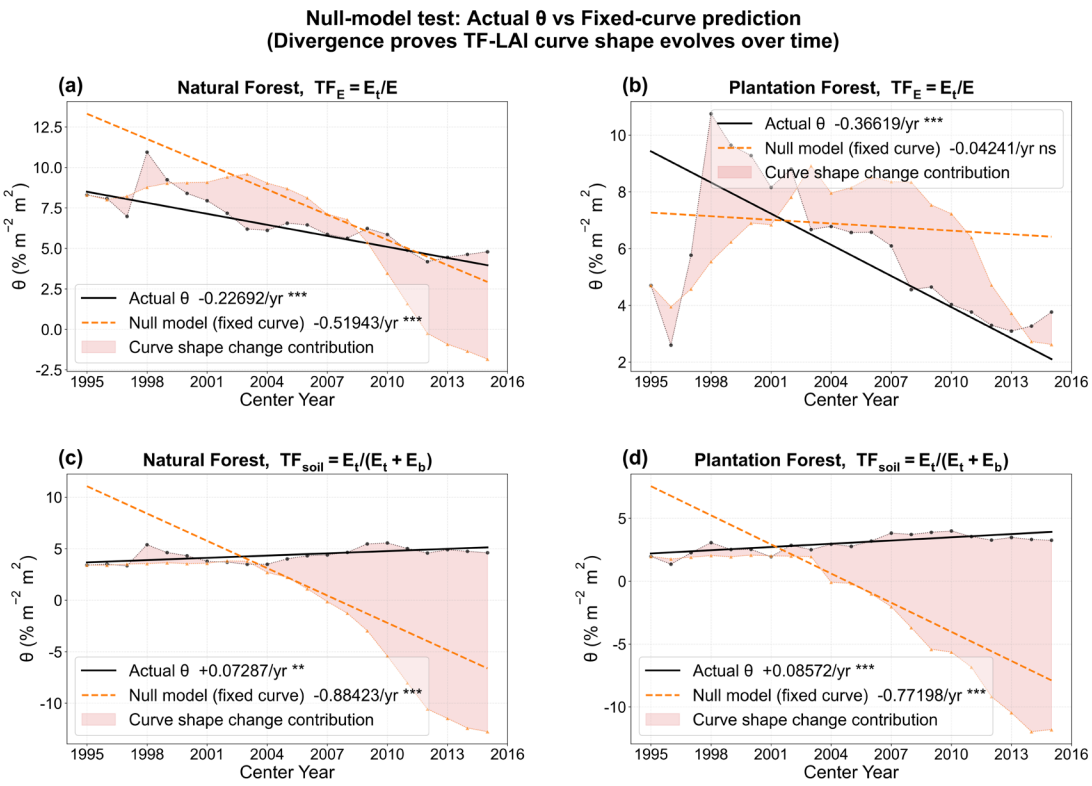

Figure S11. Null-model comparison: actual θ trajectory (blue) versus a fixed-curve null model (red dashed) that holds regression coefficients (a_0, b_0, c_0) constant at their first-window values while allowing LAI to change. TF_E (top) and TF_{soil} (bottom) shown for natural (left) and planted (right) forests. Theil–Sen slopes and Mann–Kendall significance annotated for both.

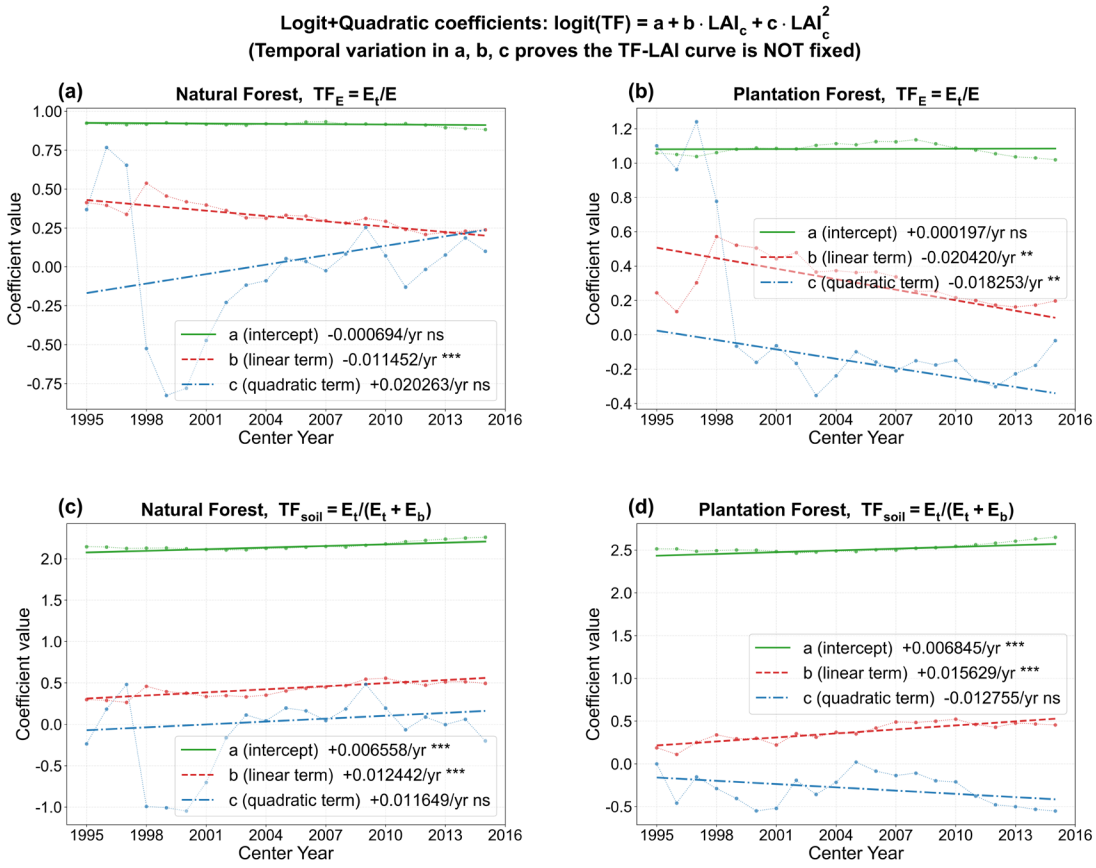

Figure S12. Temporal evolution of the logit-quadratic regression coefficients a (intercept), b (linear LAI term), and c (quadratic LAI term) for TF_E (top) and TF_{soil} (bottom), natural (left) and planted (right) forests. If the TF–LAI curve were time-invariant, all coefficients would be constant. Theil–Sen trend lines overlaid with Mann–Kendall significance. A significant trend in b directly reflects a change in the LAI–TF coupling strength.

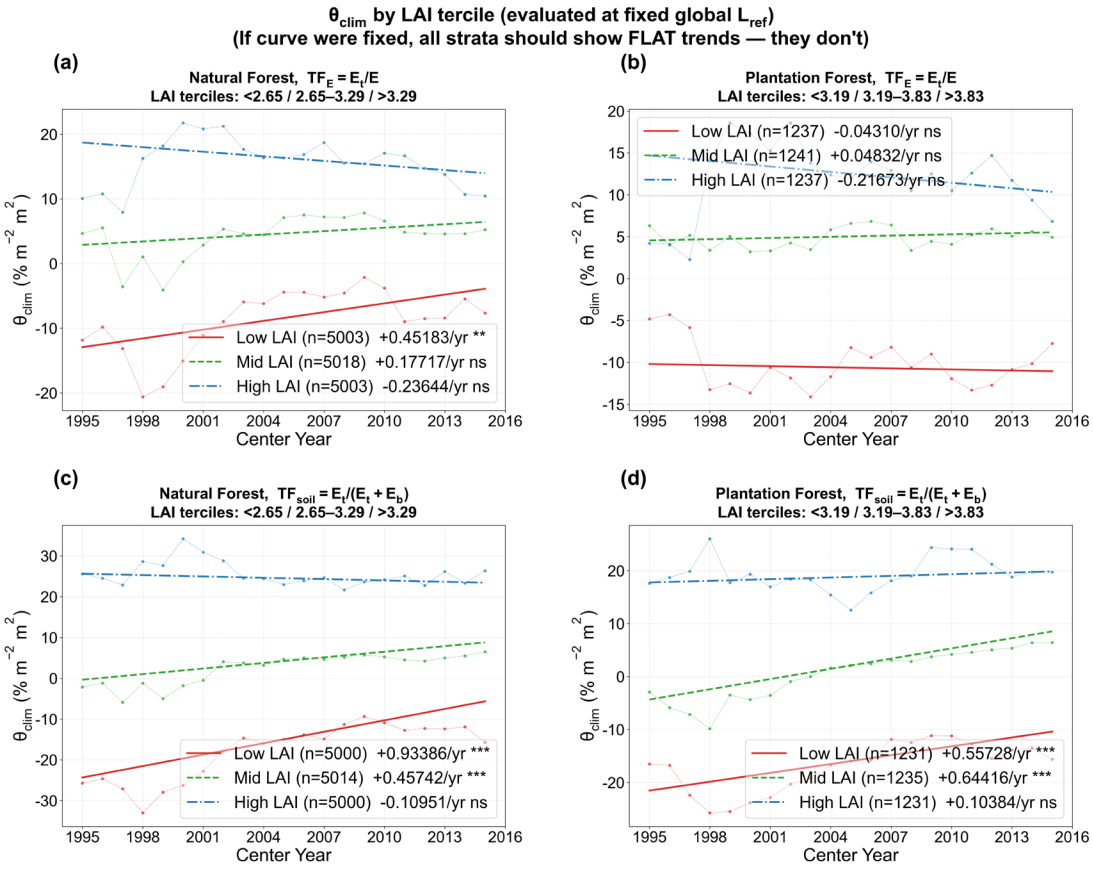

Figure S13. LAI-stratified θ_{clim} trends. Pixels are divided into three terciles by their mean LAI: Low, Mid, and High. θ_{clim} is evaluated at a global fixed LAI reference for all pixels. If the curve were fixed, all terciles would show no trend. TF_E (top) and TF_{soil} (bottom), natural (left) and planted (right) forests. Theil–Sen slopes and Mann–Kendall significance annotated. High-LAI terciles tend toward ns, partially supporting saturation, but Low/Mid terciles show significant trends under TF_{soil}.

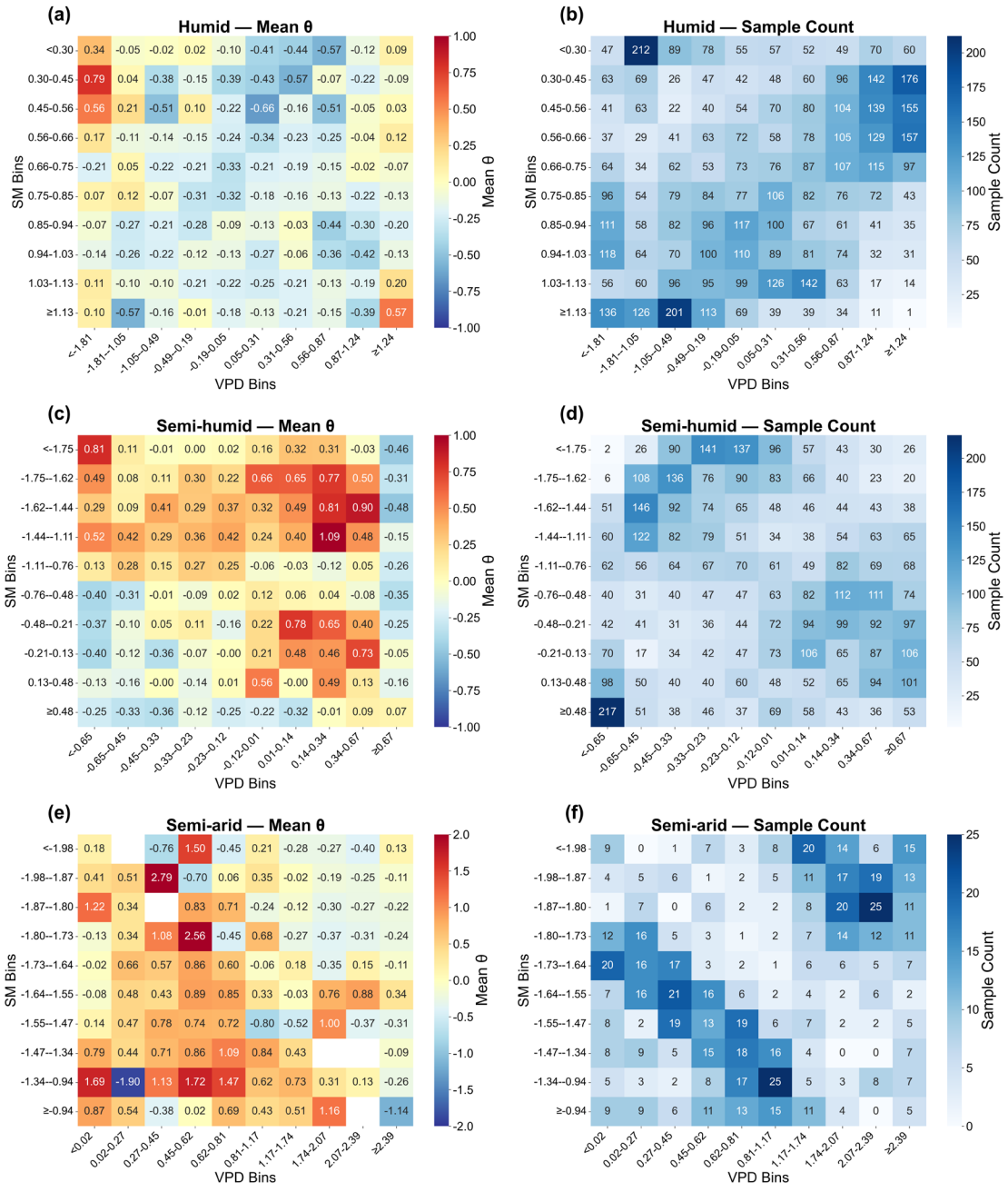

Figure S14. Pooled spatial results of forest LAI—TF sensitivity (θ) under Soil Moisture (SM) and Vapor Pressure Deficit (VPD) bins for Natural Forests in different climatic zones. (a, b): Humid zone, (c, d): Semi-humid zone, (e, f): Semi-arid zone. The left column of heatmaps shows the mean θ value within different SM and VPD combination intervals, with color indicating the magnitude of θ. The right column of heatmaps shows the data sample size within each combination interval.

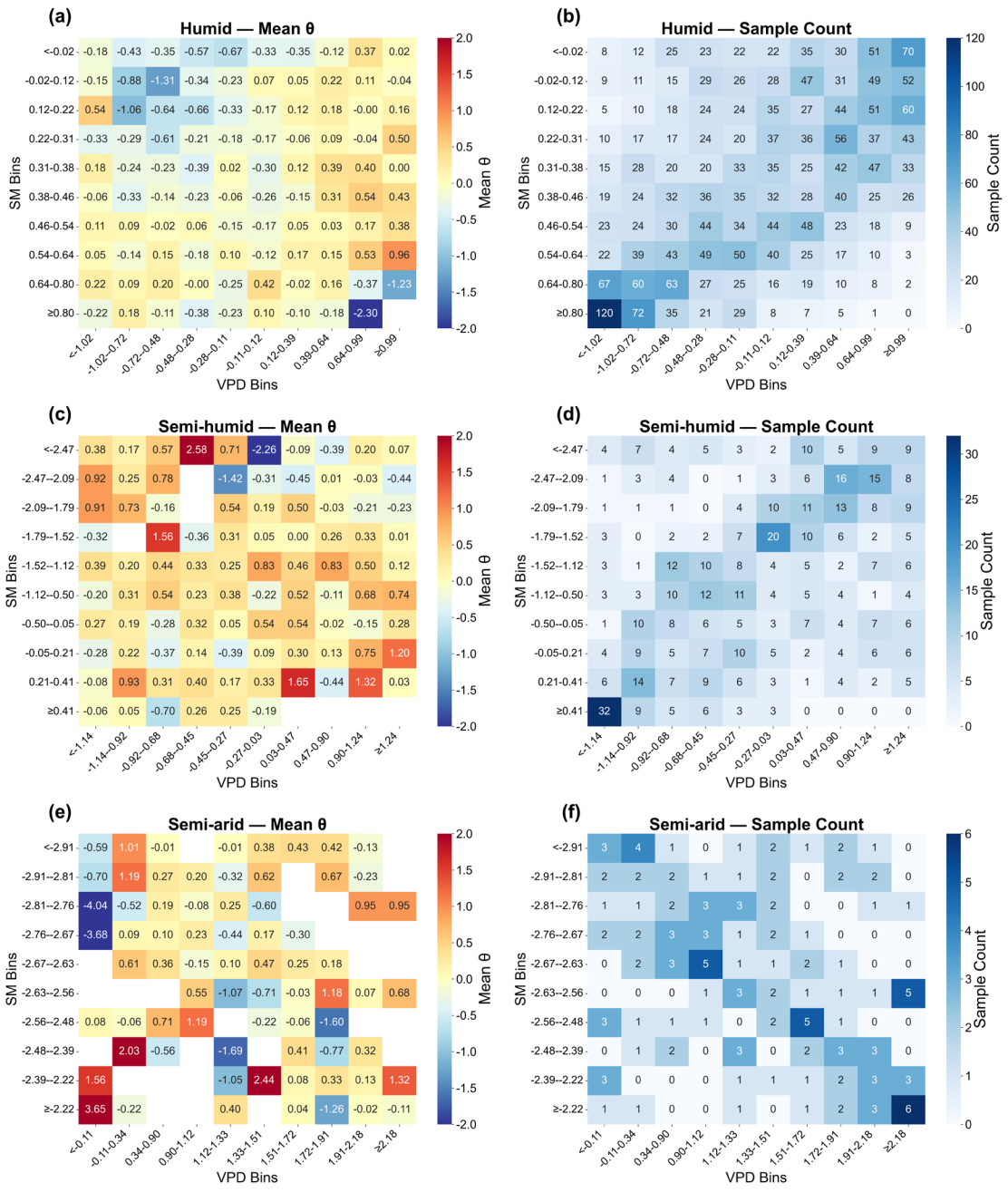

Figure S15. Pooled spatial results of forest LAI—TF sensitivity (θ) under Soil Moisture (SM) and Vapor Pressure Deficit (VPD) bins for Plantation forests in different climatic zones. (a, b): Humid zone, (c, d): Semi-humid zone, (e, f): Semi-arid zone. The left column of heatmaps shows the mean θ value within different SM and VPD combination intervals, with color indicating the magnitude of θ. The right column of heatmaps shows the data sample size within each combination interval.

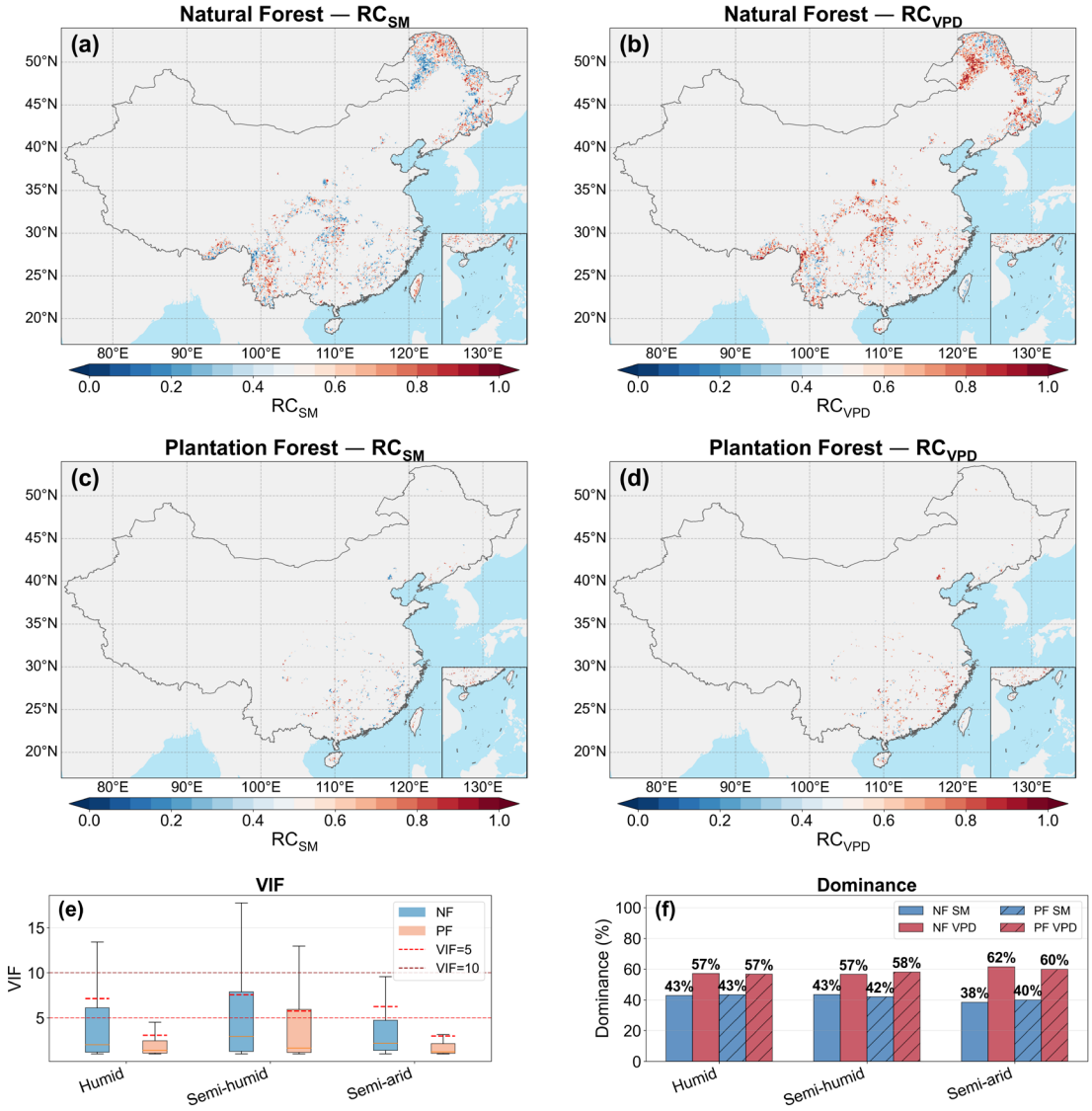

Figure S16. Spatial distribution of the relative contributions (RC) of SM and VPD to θ_{total}, together with variance inflation factor (VIF) and dominance statistics across climatic zones. RC was calculated as $|\beta_i|/(|\beta_{SM}|+|\beta_{VPD}|)$, ranging from 0 to 1. Panels (a) and (b) show RC_{SM} and RC_{VPD} for natural forests (NF), respectively, and panels (c) and (d) show the corresponding results for plantation forests (PF). Panel (e) shows VIF boxplots for NF and PF across climatic zones, with dashed lines marking VIF = 5 and VIF = 10. Panel (f) shows the proportions of SM- and VPD-dominated pixels in NF and PF by climate zone. The generally low-to-moderate VIF values indicate that multicollinearity between SM and VPD does not overturn the main ridge-regression inference.

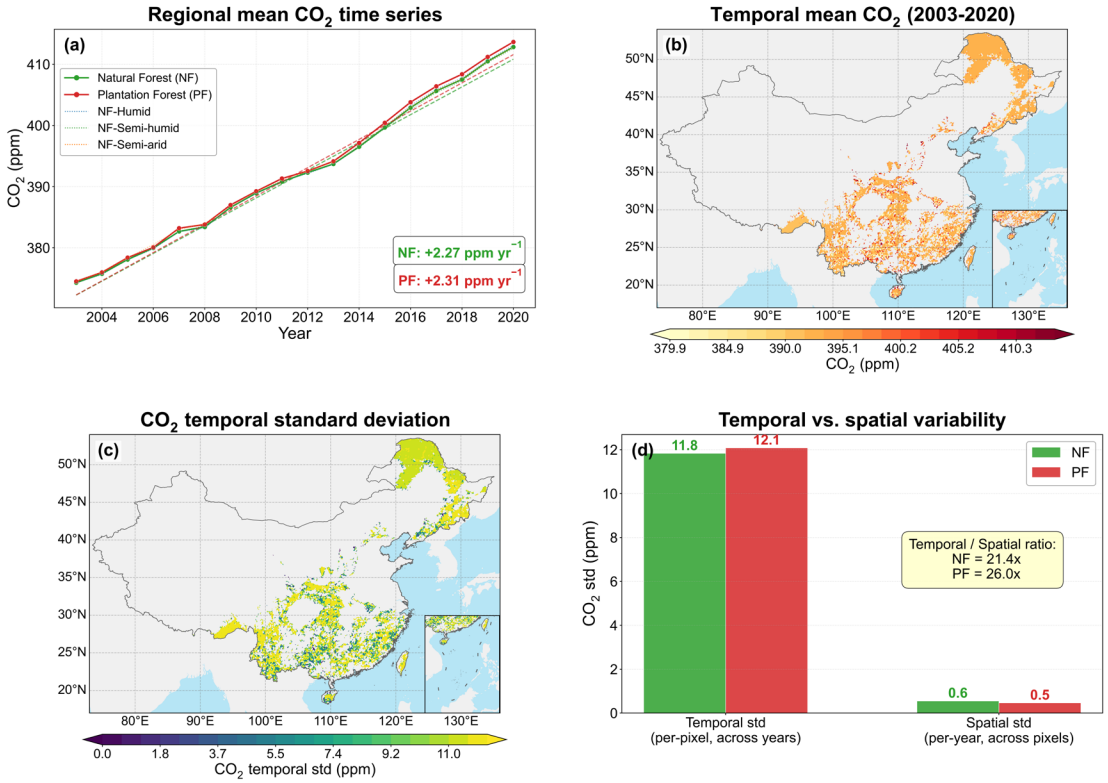

Figure S17. Spatiotemporal characteristics of atmospheric CO_2 concentration over Chinese forests (2003-2020) and the rationale for excluding CO_2 from the main pathway model. (a) Regional mean CO_2 time series for natural forests (NF, green) and plantation forests (PF, red), with Theil-Sen trend lines (dashed). Thin dotted lines show NF sub-regional means by climate zone (Humid, Semi-humid, Semi-arid). (b) Temporal mean CO_2 spatial distribution (2003-2020 average), showing limited spatial heterogeneity across the study domain. (c) Temporal standard deviation of CO_2, reflecting the magnitude of interannual variability at each pixel. (d) Comparison of temporal variability (per-pixel standard deviation across years) and spatial variability (per-year standard deviation across pixels) for NF and PF. The temporal-to-spatial ratio exceeds 20:1 for both forest types, indicating that CO_2 acts primarily as a temporally uniform background forcing rather than a spatially heterogeneous driver.

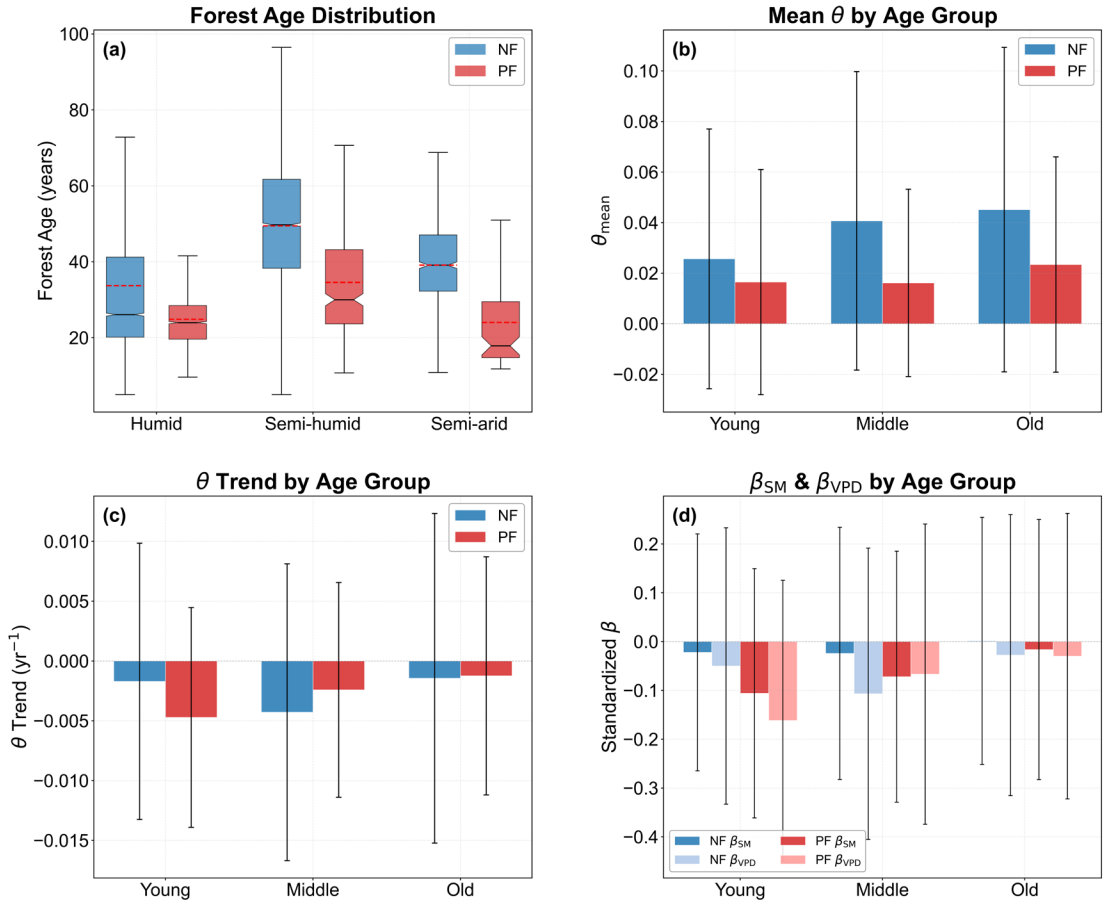

Figure S18. Comparison of LAI–transpiration fraction sensitivity (θ) between natural forests (NF) and (PF) after stand-age stratification. (a) Box plots of forest age distribution for NF and PF across climate zones. NF and PF are independently stratified into Young, Middle, and Old groups using the 33.3rd and 66.7th percentile thresholds. Boxes span the IQR; notches indicate 95% CI of the median; red dashed lines denote means. (b) Mean θ (θ_{mean}) by age group. Error bars indicate ±1 standard deviation. NF exhibits consistently higher θ than PF in all age groups, confirming that the NF > PF difference is not driven by stand-age differences. (c) θ temporal trend (θ_{trend}) by age group. Negative values indicate declining θ over 1990–2020. (d) Standardized ridge regression coefficients β_{SM} and β_{VPD} by age group. Darker bars: β_{SM}; lighter bars: β_{VPD}. The negative sign of β_{VPD} is consistent across all age groups, indicating a robust VPD suppression effect.

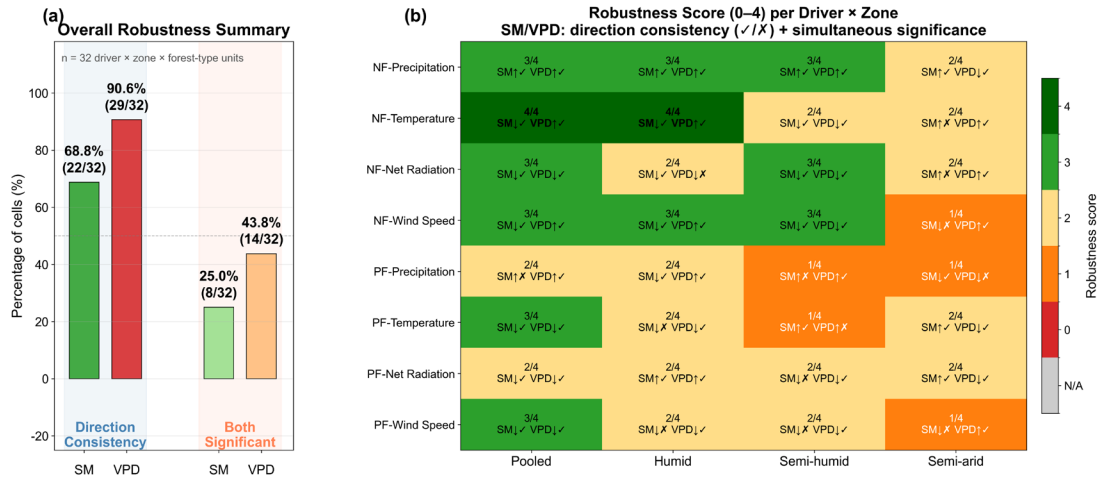

Figure S19. Robustness of pathway indirect effects to mediator specification. (a) Overall robustness summary across 32 driver × zone × forest-type units. Bars show the percentage of units with the same sign of the indirect effect between the single-mediator and joint models ("Direction consistency") and the percentage of units significant in both specifications ("Both significant") for SM- and VPD-mediated pathways. (b) Robustness score (0–4) for each driver × zone combination in natural forests (NF) and plantation forests (PF). The score combines sign consistency and simultaneous significance between the single-mediator and joint models for SM- and VPD-mediated indirect effects; higher values indicate greater robustness. Overall, VPD-mediated indirect effects were more robust across mediator specifications than SM-mediated indirect effects.

Table S1. Effects of including atmospheric CO_2 as an additional covariate in regressions of LAI–transpiration fraction sensitivity (θ_{total}).

Forest type	Zone	n	Base R^2 (SM+VPD)	Full R^2 (SM+VPD+CO_2)	ΔR^2	r(θ,CO_2|SM, VPD)	p	Significance
NF	All	13	0.3201	0.7189	0.3988	-0.7658	0.002272	**
NF	Humid	13	0.2652	0.7218	0.4566	-0.7883	0.001368	**
NF	Semi-humid	13	0.0165	0.5129	0.4964	-0.7104	0.0065	**
NF	Semi-arid	13	0.1647	0.3304	0.1656	-0.4453	0.127314	
PF	All	13	0.5153	0.8462	0.3309	-0.8262	0.000499	***
PF	Humid	13	0.3784	0.8135	0.4351	-0.8366	0.000363	***
PF	Semi-humid	13	0.0413	0.8056	0.7642	-0.8929	0.00004	***
PF	Semi-arid	13	0.1739	0.7907	0.6168	-0.8641	0.00014	***

n = number of overlapping center years (2003–2015) from the zone-mean time series. Base R^2: coefficient of determination from the ordinary least squares (OLS) regression of θ on SM and VPD; Full R^2: coefficient of determination from the OLS regression of θ on SM, VPD, and CO_2.; ΔR^2 represents the R^2 increase from including CO_2. r(θ, CO_2|SM, VPD) is the partial correlation between θ and CO_2 after controlling for SM and VPD. The substantial increase in R^2 likely reflects the fact that CO_2 shares strong temporal trends with θ, rather than acting as a spatially heterogeneous driver. This result is therefore consistent with excluding CO_2 from the main pixel-level pathway model. Significance levels: ***p < 0.001, **p < 0.01, *p < 0.05.

Table S2. Summary of standardized regression coefficients and model fit for θ before and after including stand age as a covariate.

Forest type	zone	n	Base β_{SM}	Full β_{SM}	$\Delta\beta_{SM}$ (%)	Base β_{VPD}	Full β_{VPD}	$\Delta\beta_{VPD}$ (%)	β_{Age}	Base R^2	Full R^2
NF	All	14799	0.018596	0.018562	-0.18146	-0.0261	-0.02617	0.268319	-0.00022	0.001406	0.001406
NF	Humid	7590	0.069857	0.06723	-3.76057	-0.00622	-0.01485	138.826	-0.03061	0.005259	0.006132
NF	Semi-humid	6427	-0.02205	-0.00042	-98.0811	-0.05869	-0.01285	-78.0976	0.084838	0.002495	0.008224
NF	Semi-arid	782	0.063513	0.054823	-13.6813	0.107623	0.074802	-30.4965	-0.07905	0.006091	0.011584
PF	All	3665	0.016703	0.018508	10.80832	0.085037	0.09244	8.705592	0.067853	0.006136	0.010695
PF	Humid	2952	-0.06459	-0.05787	-10.4064	0.037479	0.046368	23.71681	0.060977	0.008436	0.0121
PF	Semi-humid	575	0.101226	0.103124	1.87446	0.134909	0.141486	4.874532	0.01984	0.008914	0.009279
PF	Semi-arid	138	0.131686	0.227455	72.72534	0.217689	0.25655	17.85157	0.291398	0.057023	0.132254

Each row reports regression results for a specific forest type × climate zone. Forest type: NF = natural forest, PF = plantation forest; Zone: All = entire domain, Humid / Semi-humid / Semi-arid = climate zone; *n* = number of valid pixels used in the regression; Base β_{SM} and Base β_{VPD} are the standardized regression coefficients for soil moisture (SM) and vapor pressure deficit (VPD) from the baseline model; Full β_{SM} and Full β_{VPD} are the corresponding coefficients from the model including stand age; $\Delta\beta_{SM}$ (%) and $\Delta\beta_{VPD}$ (%) denote the percentage changes in the standardized coefficients after including stand age; β_{Age} is the standardized regression coefficient for stand age; Base R^2 and Full R^2 are the coefficients of determination for the baseline and full models, respectively. All variables were z-score standardized before OLS regression (with intercept). Zone-level regressions used zone-specific z-score standardization.